HEAT REQUIREMENTS FOR FIXED BED PYROLYSIS OF WOOD

J. Ábrego*, M. Atienza-Martínez, F. Plou, J. Arauzo

Thermochemical Processes Group (GPT), Aragón Institute for Engineering Research (I3A), Universidad de Zaragoza, Edificio I+D, C/ Mariano Esquillor s/n, 50018 Zaragoza, Spain

**Corresponding Author: Telephone +34876555483 e-mail: abrego@unizar.es*

Abstract

In this work, the evolution of heat during the pyrolysis of dry wood chips has been experimentally measured in an externally heated fixed bed reactor. Heat requirements for pyrolysis (Q_P) are reported as a function of the central bed temperature, and the occurrence of exothermic and endothermic events, linked to the decomposition of the biomass individual constituents, is verified. The different thermal behavior of a fixed bed of pyrolyzing wood when applying slow or high heating rates is distinguished, and the enthalpy of the pyrolysis reactions (ΔH_P) is estimated. The results show good coincidence with the previously reported literature values.

Keywords: Biomass pyrolysis; heat for pyrolysis

1. Introduction

The design of pyrolysis reaction systems that can efficiently convert abundant biomass resources into valuable products is a subject of growing interest [1]. Pyrolysis is a versatile technology for biomass conversion that can be directed towards obtaining a major solid product fraction (biochar), a liquid fraction (bio-oil) or both.

The practical importance of thermal (endothermic and/or exothermic) effects during the pyrolysis of biomass was well known in the wood distillation industry, although the details of such effects have only been clarified recently. Antal and Grönli [2] extensively reviewed the pioneering works on this matter —dating back to the 19th Century—, and provided a detailed explanation of the reaction conditions that favor certain exothermic effects in pyrolysis. They showed that char formation by secondary heterogeneous reactions is strongly exothermic, and that these secondary reactions are favored if high pressure and high volatile residence time (i.e., high volatile concentrations and low flowrates) are applied. Apart from secondary interactions, Di Blasi et al. [3] recently reviewed the primary decomposition reactions that

contribute to pyrolysis exothermicity. They established that a first stage of exothermicity proceeds because of hemicellulose decomposition, followed by an endothermic or thermally neutral stage caused by the mixed contributions of cellulose and lignin degradation, and a third exothermic stage attributed to lignin decomposition.

Given that pyrolysis reaction heats are inherently linked to the decomposition of biomass constituents and therefore with pyrolysis product distribution, it is clear that the evaluation of heat of pyrolysis reactions is of great importance from the point of view of reactor design [4]. Additionally, for the pyrolysis reactions to take place, it is needed an initial supply of external heat to reach high enough temperatures to enable the decomposition reactions of the biomass components [5]. The total amount of heat that needs to be supplied is usually called heat *for* pyrolysis (i.e. the total energy consumed during pyrolysis, including sensible enthalpy and enthalpy of reaction), whereas heat *of* pyrolysis is the net reaction enthalpy for the multitude of individual chemical reactions. Both terms, used in this work, follow the proposed definitions by the IEA Bioenergy Pyrolysis Activity [6]. Hereinafter, they will be referred to as Q_P and ΔH_P, respectively.

Table 1. Some reported values for the energy requirements of pyrolysis.

Energy requirements for pyrolysis		Material	Remarks	T(ºC)	Reference
Given value	(kJ/kg dry feed)				
Q_P	780–1640[a]	Oak, pine, corn stover, oat hulls	Heat balance in a fluidized bed reactor, including heat loss estimation	500	Daugaard and Brown [7]
Q_P	2909–3472	Birch	"Water tracer technique", large particles (dowels)	>700	Reed and Gaur [8]
Q_P	249–400	Beech	Heat balance in a screw torrefaction reactor, including heat loss estimation	270–300	Ohliger et al. [9]
ΔH^0_P	-199–148				
Q_P	2020	Cashew nutshells	Heat balance using experimental data of a pyrolysis reactor	500	Ábrego et al. [10]
ΔH^0_P	470		Estimation of enthalpy of vapor products according to [11]		
Q_P	1100–1600	Cedar, pine, willow, bamboo	Heat balance, using data of a screw pyrolyzer, including estimation of enthalpy of vapor products.	500–550	Yang et al. [11]
Q_P	389–600[a]	Pine, cotton stalk, peanut shell and wheat straw	DSC, with lid on crucible. Direct integration of DSC curve	167–700	He et al. [12]
Q_P	207–434[a]	Spruce, eucalyptus, poplar, sawdust, corn, sunflower, straw and sewage sludge	DSC (no info about lid use). Direct integration of DSC curve	500	Van de Velden et al. [13]
Q_P	-79	Pine	DSC (no info about lid use). Direct integration of DSC curve	500	Bilbao et al. [14]
Q_P	-140–2678	Olive mill waste	DSC, with/without lid on crucible. Direct integration of DSC curve	600	Manyà et al. [15]
Q_P	1400–2000	Meat and bone meal	Heat balance in a fluidized bed reactor, including heat loss estimation	450–600	Berruti et al. [16]
Q_P	800–3300	Grape residues		300–600	Xu et al. [17]
Q_P	763–3129	Oak	Heat balance of industrial furnace, using lab-scale fixed bed data, using compositional formulas and HHVs of biomass and products	500–1100	Kodera and Kaiho [18]
ΔH^0_P	-(2872–3378)				
ΔH^0_P	-500–1500	Cedar	Heat balance using data from a fluidized bed reactor	450–650	Hosokai et al. [19]
ΔH^0_P	-1100–800	Sewage sludge	Heat balance using experimental data of various combinations of torrefaction and pyrolysis stages	530-550	Ábrego et al. [20] Atienza-Martínez et al. [21]

ΔH_P	933–1323	Pine, spruce, birch, beech	Heat balance using data from fixed bed pyrolysis	400	Klason [22]
ΔH_P	-(160–240)	Wood, various	Review of various previous estimations at different conditions	>350	Roberts [23]
ΔH_P	-222–128	Beech and spruce	DSC, with/without lid on crucible. Subtraction of sensible heat from solids heating	500	Rath et al [24]
ΔH_P	-250–0	Beech	Deduced from single particle model and experiments using a wood cylinder	200-280	van der Stelt [25]
ΔH_P	-283–175	Corn stalks and various wood species	DSC, with/without lid on crucible. Subtraction of sensible heat from solids heating Operating pressures: 0.1 and 2.0 MPa	550	Basile et al. [26]
ΔH_P	-68–222	Beech and thistle	DSC, with/without lid on crucible. Subtraction of sensible heat from solids heating	550	Gómez et al. [27]
ΔH_P	-859–620	Poplar, pine bark, rice straw, corn stalk	DSC, with/without lid on crucible. Subtraction of sensible heat from solids heating	500	Chen et al. [28]

[a] The evolution of Q_P with temperature was calculated. Values in the Table correspond to T=500 ºC.

There have been different approaches to determine the energy requirements of biomass and waste pyrolysis. Some of them are summarized in Table 1 (literature values reported as a result of fitting of model parameters are not considered). At a first glance, it can be seen that the significantly different pyrolysis temperatures, biomass materials and conditions (reactor type, heating mode, particle size, inert medium, residence time of volatiles and heating rate, amongst others) may partly explain the enormous variability of the reported values for the energy requirements of pyrolysis. Moreover, these results also differ in the estimation method applied, and thus values presented in Table 1 are further classified (Q_P, ΔH^0_P or ΔH_P) according to the diagram presented in Figure 1, that shows graphically that caution must be taken when comparing these values [29].

Indeed, the main difficulties that arise when trying to estimate ΔH_P values from experimental data are related to the difficulty of estimating sensible heats of the condensable vapors and, in a lesser extent, those of the chars and/or unconverted biomass. In this regard, a relevant contribution on the estimation of thermal properties of the vapors has been done by Yang et al. [11] with the development of equations that accurately predict the standard enthalpy of formation and sensible heats of bio-oil vapors at a given temperature, as a function of their elemental composition. Several contributions on the estimation of specific heat (c_p) of biomass and chars as a function of temperature can also be found in the literature [30–33]. However, (i) for raw biomass, care must be taken in employing dedicated correlations for each type of biomass species because of relatively high variabilities [33], and (ii) for chars, even higher variabilities are also found (that can be partly attributed to the different biomasses, particle sizes, final temperatures and reactor systems used for char production). Moreover, an important issue for chars is that in most cases the published correlations are only valid in low temperature ranges (generally below 350 ºC), and thus require

extrapolation at higher temperatures [28], which adds more uncertainty [9]. Perhaps because of this reason, correlations for specific heat of coal chars covering higher temperature ranges have been sometimes used [24], although the estimation errors can be significant.

Probably, the most straightforward way for obtaining Q_P and ΔH_P involves the use of a TGA-DSC system, that is capable of determining both the mass loss and heat flux curve of the pyrolysis process, and the specific heat of biomass and chars in separate experiments. However, the use of this technique requires experimental conditions that are significantly different from those of practical applications, such as small sample amounts, small particle sizes or high inert gas flowrates. Thus, in some cases the obtained values may not realistically represent the thermal behavior of pyrolysis reactors, in which significant heat and mass transfer effects are present [34,35]. Moreover, only qualitative differences can be found when studying the influence of secondary pyrolysis reactions, because using (or not) a lid over the sample crucible is the only method available to control the residence time of the evolved volatiles within the system. Finally, it may be also necessary to account for the radiative heat effects, especially when lids are not used on the DSC crucibles [24].

To overcome these limitations, it would be desirable to develop a simple experimental system and method capable of estimating Q_P, ΔH^0_P and/or ΔH_P under practical pyrolysis conditions, trying to avoid as much as possible the use of literature data that might not be representative of the specific case addressed. In order to achieve this objective, the experimental system should be able to measure the evolution of temperatures and heat input during pyrolysis, and at the same time determine the final product yields (char, water, bio-oil and gases) and their characteristics. Such a system would benefit from the combination of the advantageous features of both TGS-DSC and experimental systems for the determination of the heat requirements of pyrolysis. The present work aims to contribute to this goal by presenting the results obtained in a novel experimental fixed bed pyrolysis system that works as a heat balance calorimeter, employing wood chips as raw material.

To the best of our knowledge, this is the first report of the evolution of heat in a fixed bed laboratory reactor as a function of temperature and based on direct experimental measurements, identifying and quantifying the successive exothermic and endothermic effects and their direct relationship to the decomposition of the individual components of wood. The experimental results allow to hypothesize the different thermal behavior of a fixed bed of pyrolyzing wood when applying slow or high heating rates, and to estimate the enthalpy of pyrolysis accordingly.

2. Materials and Methods

2.1. Raw Material.

Beech wood chips, commonly used in biomass pyrolysis studies [36,37], were the raw material used in the experiments. The size range of the wood chips was approximately 4-16 mm. Proximate analysis, ultimate analysis and higher heating value measurements are shown in Table 2. Previously to each experiment, the biomass samples were dried in an oven at 105 ºC overnight.

Table 2. Proximate/ultimate analyses, higher heating value (HHV) of the raw material.

	analytical standard	units	Value
moisture	ISO-589-1981	wt. %	11.29
ash	ISO-1171-1976	wt. %	0.28
volatiles	ISO-5623-1974	wt. %	78.55
fixed carbon	[a]	wt. %	9.88
C	[b]	wt. %	43.52
H[c]	[b]	wt. %	5.77
N	[b]	wt. %	0.04
S	[b]	wt. %	n.d.
O	[d]	wt. %	50.34
HHV[e]	ISO-1928-2009	$MJ \cdot kg^{-1}$	17.0

[a] By difference. [b] Ultimate analysis was performed using LECO Truspec. [c] The wt. % of hydrogen contents moisture hydrogen. [d] oxygen (wt. %) = 100 – carbon (wt. %) – hydrogen (wt. %) – nitrogen (wt. %) – sulfur (wt. %) – ash (wt. %). [e] HHV was determined using IKA C 2000 Basic Calorimeter.

2.2. TGA-DSC analyses.

Thermogravimetric analysis (Netzsch STA 449 TGA) was performed using single, whole beech wood chips without prior drying, which were placed in a crucible covered with a lid. A nitrogen flow of 100 $mL \cdot min^{-1}$ was employed as inert gas atmosphere. The heating rate applied was 10 $ºC \cdot min^{-1}$. The system was previously calibrated under these same operational conditions. Three replicates were done with good reproducibility.

2.3. Experimental lab-scale pyrolysis system and procedure.

The biomass pyrolysis experiments were performed in a laboratory-scale batch fixed bed reactor. The layout of the system is shown in Figure 2.

The pyrolysis reactor can hold around 100 g of beech wood chips. In each experiment, heating of the pyrolysis reactor is accomplished by means of an outer annular vessel that contains 1000 g of silica sand. Previously to the beginning of the pyrolysis experiment, the sand bed is heated up to a predefined temperature (T_{S0}) by a well-insulated electrical furnace. The sand bed thermocouple is placed at the mean diameter and height of the annular bed. The position of this thermocouple was set according to preliminary experiments that showed that the uniform electrical heating did not produce significant vertical temperature gradients within the sand bed. Additionally, and due to the small thickness of this annular sand bed (around 10 mm), uniform radial temperatures were assumed.

Once T_{S0} is reached for the sand bed, the electrical heating is disconnected, the pyrolysis reactor is inserted in the inner zone and the vapor outlet is connected to the liquid collection and gas sampling systems. At this moment (t = 0) the experiment begins and the temperature of the biomass bed (T_P) is registered by means of a thermocouple placed at its center (r = 0) and at 1/3 of the reactor height from its bottom. This height was chosen because of the expectable gradual volume reduction in the biomass bed because of thermal decomposition. The final pyrolysis temperature (T_{Pf}) is taken as the maximum temperature reached by the biomass bed. During the experiment, the temperature of the silica sand bed (T_S) is also continuously registered. The experiments are considered to end when both the biomass and the sand bed have reached similar temperatures and show a consistent temperature decrease, evidencing that no additional biomass decomposition is taking place inside the reactor. The typical duration of a pyrolysis experiment in the reaction system is around 30 minutes.

During the experiments, no carrier gases are used. The liquid collection system comprises two ice-cooled condensers and a cotton filter. The gas composition is continuously measured with a gas micro-chromatograph (Agilent 3000A). The solid and liquid yields are calculated, and gas yield is determined by difference. Water content of liquids is determined by Karl-Fischer titration (Mettler Toledo V-20 Analyzer). The higher heating value of solids and liquids is measured by means of a calorimeter (IKA C 2000). Ultimate analysis are performed using LECO Truspec.

Five different starting temperatures were chosen for the silica sand bed: 400, 500, 600, 700 and 800 ºC. At these temperatures, both pyrolysis and ‘blank’ experiments (empty reactor) were made. Blank experiments are required since they are necessary to know how the pyrolysis reactor is heated up in the absence of biomass pyrolysis reactions. In this case, the reactor is only filled with air, and it is assumed that the air inside the reactor is always at a uniform temperature. All these experiments (blank and pyrolysis) were

replicated. Finally, additional validation experiments were performed to verify the adequateness of the estimation procedure, using a measured amount of a reference material with well-known specific heat (aluminum).

Hereafter, the different types of experiments are referred to using letters (B: blank, P: pyrolysis). Each individual pyrolysis experiment is referred to as P followed by the starting temperature of the sand bed (e.g. P400 for the experiment with an initial sand bed temperature of 400 ºC).

2.4. Estimation of heat for pyrolysis. Q_P.

For each starting sand bed temperature, heat for pyrolysis is estimated as the difference between the heat released by the silica sand bed in the pyrolysis and the blank experiments, respectively. The estimation is based on a simple energy balance as follows. At any moment in the blank experiments, the heat released by the silica sand ($Q_{S,B}$) is partly employed to heat the empty reactor ($Q_{reactor}$), and partly lost to the surroundings (Q_{losses}), as shown in Equation 1. The sand (mass m_S and specific heat $c_{P,S}$) is cooled from T_{S0} to $T_{S,B}$, while the reactor is heated up to T_P:

$$Q_{S,B} = m_S \cdot \int_{T_{S0}}^{T_{S,B}} c_{P,S} \cdot dT = Q_{reactor}(T_P) + Q_{losses} \qquad \text{Equation 1}$$

In the pyrolysis experiments, the heat released by the sand bed ($Q_{S,P}$) is also employed to heat up and pyrolyze the bed of biomass; thus, when the reactor reaches a temperature T_P, the temperature of the sand bed ($T_{S,P}$) will be different from that one from the previous case, as shown in Equation 2:

$$Q_{S,P} = m_S \cdot \int_{T_{S0}}^{T_{S,P}} c_{P,S} \cdot dT = Q_{reactor}(T_P) + Q_P + Q_{losses} \qquad \text{Equation 2}$$

Assuming that the heat losses will be similar in both cases, the subtraction of both equations allows estimating the heat for pyrolysis solely as a function of the temperature variation and specific heat of the silica sand, as shown in Equation 3:

$$Q_P = Q_{S,P} - Q_{S,B} = m_S \cdot \int_{T_{S,P}}^{T_{S,B}} c_{P,S} \cdot dT \qquad \text{Equation 3}$$

In this work, Q_P was evaluated within a temperature interval comprising the beginning of each pyrolysis experiment to the final pyrolysis temperature attained (T_{Pf}), which is determined in each individual experiment. Values of heat capacity for sand are taken from the HSC Chemistry software database [38].

2.5. Estimation of heat of pyrolysis, ΔH_P.

The difference between Q_P and ΔH_P is the sensible heat required by the biomass material. Therefore, ΔH_P can be estimated by adapting the approximation applied by Rath et al. [24] for TGA-DSC data, that allows

to estimate sensible heat required for pyrolyzing biomass. A dimensionless conversion for biomass can be defined:

$$X(T) = \frac{m_0 - m(T)}{m_0 - m_f} \quad \text{Equation 4}$$

where m_0 is the initial weight of biomass inside the reactor, $m(T)$ is the remaining fraction at a given temperature, and m_f is the final char mass of each experiment. A sensible heat curve can then be built by calculating [24]:

$$Q_S(T) = \int_{T_0}^{T} [(1 - X(T)) m_0 c_{P,wood} + X(T)) m_{char} c_{P,char}] dT \quad \text{Equation 5}$$

Instead of using TGA-DSC data, in this work, Equations 4 and 5 are applied to the char yields determined in the experiments P400 to P800, in order to estimate $Q_S(T)$. This approach is adopted because char yields from TGA-DSC and from the fixed bed reactor are expected to be significantly different, and hence the sensible heat curves. Linear correlations for specific heat of beech wood and its char ($c_{p,wood}$, $c_{p,char}$) can be found in the work by Dupont et al. [33]. These correlations are valid only for up to 300 ºC; however, and according to other correlations reviewed by Hankalin et al. [31], the linear behavior extends beyond these temperature limits, with values very similar to those obtained through extrapolation of the formulae by Dupont et al. Therefore, it seems reasonable to use the formulas by Dupont et al. throughout the entire temperature range considered in this work. Ohliger et al. [9] took a similar approach, with averaged heat capacity (of char coal) and extrapolated heat capacity of wood above 150 ºC.

2.6. Validation of the experimental system.

The simplicity of the proposed method has the following potential drawbacks: the assumption of similar heat losses in the pyrolysis and blank experiments, an uneven temperature distribution in both the sand and biomass beds, as well as other experimental uncertainties, could lead to significant estimation errors. Thus, in order to validate the proposed experimental system and procedure, some sort of experimental validation was required.

In the validation experiments performed, a mass of 100.0 g of aluminum was placed into the reactor, and heated in the same conditions as in the blank and pyrolysis experiments. Aluminum was chosen because its high thermal conductivity allows assuming homogeneous temperatures through the sample, and for its known values of specific heat in the temperature range tested. These values were taken from HSC Chemistry software. Results of the validation experiments can be found in the Supplementary Information Section, and the experimental error was found to be within 10% at the end of each experiment in all cases.

3. Results and Discussion

3.1. TGA-DSC analysis.

Thermogravimetric data are presented in Figure 3a and are in accordance to previous results reported elsewhere with a similar biomass material [39]. The drying stage of wood extends up to around 170 ºC. Significant mass loss attributable to decomposition reactions begins at around 200 ºC and increases dramatically at 250 ºC. The main mass loss stage concludes around 370 ºC and overlaps with an exothermic stage, as revealed by the DSC curve, in the interval between 270 and 445 ºC. Afterwards, a brief endothermic stage can be seen up to around 515 ºC, and another exothermic interval begins. We recall that DSC results are highly dependent on the experimental setup: on the absence or presence of a lid that retains volatiles (especially at high temperatures), mass of sample, gas flowrate, crucible material, heating rate and sample holder [40]. This case corresponds to the thermal decomposition of a single wood chip using a lid; thus, it can be seen as pyrolysis conditions in which a low gas flowrate is present, where intraparticle residence time of vapors is extended, and where extraparticle events (secondary reactions, heat or mass transfer) are mostly absent.

Figure 3b presents the evolution of heat for pyrolysis (Q_P) as determined by direct integration of the heat flow curve given by DSC. The combination of exothermic and endothermic stages as described in Figure 3a are reflected in Q_P, which shows a maximum of 400 $kJ \cdot kg^{-1}$ at 270 ºC and a steep decrease to almost 0 $kJ \cdot kg^{-1}$ at the end of the temperature range. A very similar thermal behavior has been recently reported for spherical samples of birch wood [41].

3.2. Pyrolysis temperatures.

The evolution of temperatures (sand and biomass beds, T_S and T_P) during the pyrolysis experiments in the fixed bed reactor is shown in Figure 4. According to previous studies, the temperature measurement in the center of the reactor allows a better visualization of the reaction heat effects on the temperature profile [37]. It can be seen that the higher the initial sand temperature, the higher maximum pyrolysis temperatures and heating rates are achieved, and that there are no evident temperature overshoots, in contrast to previous works [37] using an inert gas flow.

Interestingly, for P400 and P500, the final temperatures of the char bed are very similar (slightly above 300 ºC), despite the different initial sand temperatures of 400 and 500 ºC. This fact suggests the existence

of an endothermic stage at these final pyrolysis temperatures. On the other hand, experiment P400 reaches final temperatures very close to the external sand bed temperatures (about 25 ºC difference), which can be indicative of exothermic processes before the aforementioned endothermic stage. Therefore, for both experiments P400 and P500, the high experimental errors can be attributed to the occurrence of sequential exothermic and endothermic effects in a narrow temperature range. The rest of the experiments show smaller experimental error between replicates.

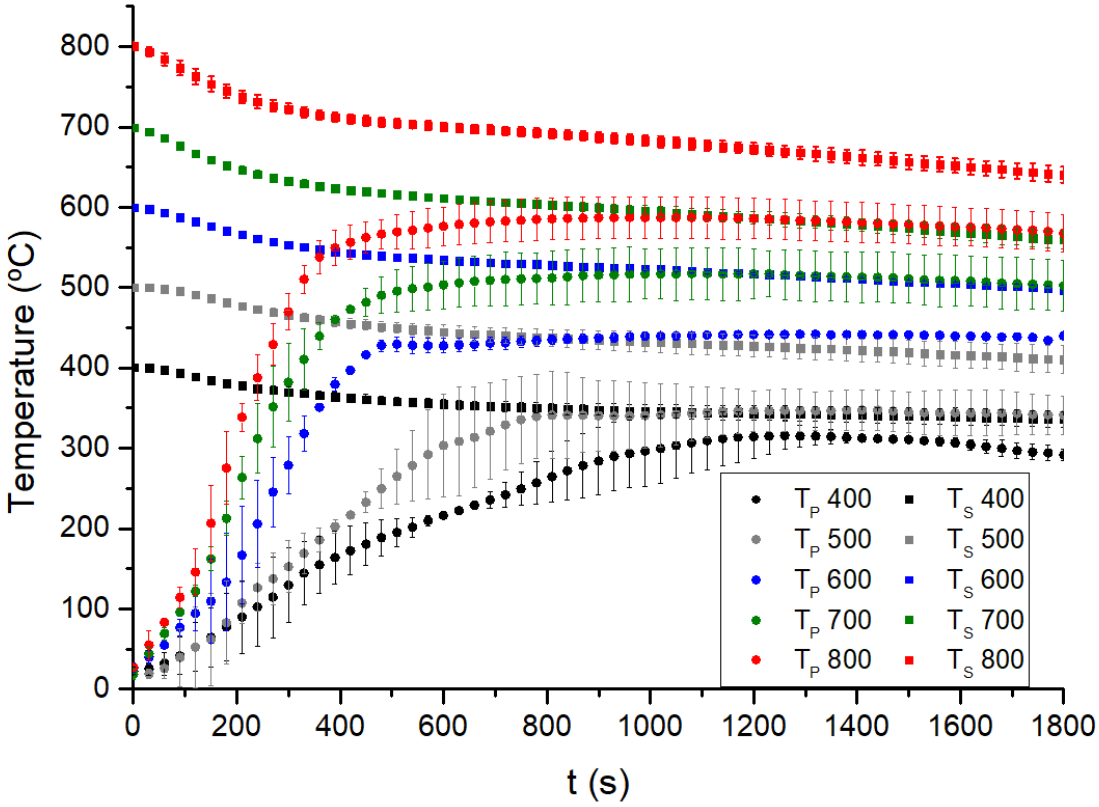

Figure 4. Evolution of the biomass bed temperatures (T_P) and sand bed temperatures (T_S) during the pyrolysis experiments (P400 - P800).

In the curves shown in Figure 4, it is difficult to determine the final pyrolysis temperature (T_{Pf}). In all the curves, a maximum temperature can be found, although it is unclear if these maxima are achieved because of pyrolysis itself, or because of unreactive heating of the resulting char after pyrolysis reactions take place. In other words, T_{Pmax} and T_{Pf} do not necessarily coincide. The maximum temperature is attained at very low heating rates at the end of each experiment. At these final stages of pyrolysis and in the absence of high temperature overshoots, bed temperatures at different radial positions are expected to become very similar, as noted by Di Blasi et al [37].

In Figure 5, the time derivative of pyrolysis temperature dT_P/dt is plotted against T_P. In general, heating rates increase after an initial stage of residual moisture evaporation. Excluding this moisture evaporation, the approach taken by Di Blasi et al. [37] was also assumed here: local maxima and minima in the heating rate can be associated with exothermic and endothermic reactions, respectively. All curves from P400 to P800 show a maximum at around 225 ºC, which is in accordance to the lower limit of the range (227-277 ºC) reported by the mentioned work of Di Blasi et al. in similar experimental conditions using beech wood and with the beginning of the observed exothermicity that peaks at around 270 ºC in the TGA-DSC results (Figure 3). At higher temperatures, the lower derivative values reveal an endothermic behavior, followed by a small shoulder above 400 ºC that may indicate another region where exothermic effects are manifest. This region has been also described in the literature [3], albeit in this work it is less pronounced and shifts to somewhat higher temperatures.

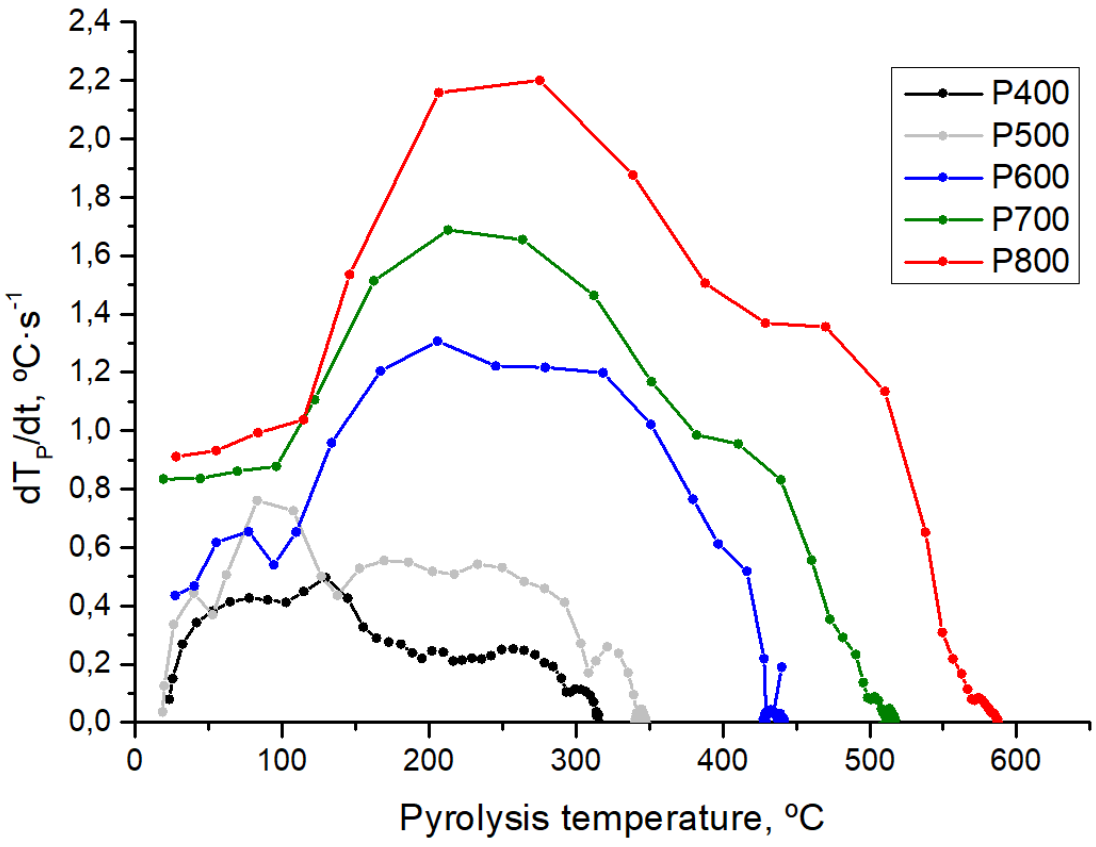

Figure 5. Evolution of the time derivative of pyrolysis temperature dT_P/dt during pyrolysis.

The maximum pyrolysis temperatures recorded in the biomass bed (T_{Pmax}) for each experiment are summarized in Table 3, as well as final pyrolysis temperatures (T_{Pf}, as determined from Q_P curves shown

below). A ratio between the final pyrolysis temperature and the initial sand bed temperature (T_{Pf}/T_{S0}) is also presented. This value can be seen as a rough indicator of how efficiently the combination of external heating and exothermic effects impacts the final pyrolysis temperature. Indeed, the presence of a minimum value for P500 (0.66) suggests that the second exothermic stage, evidenced by the mentioned shoulder in Figure 5, has not been attained in this experiment. Moreover, it can be seen in Table 3 that an increase in T_{S0} of 100 ºC (P400 to P500) causes an increase of only 45 ºC in T_{Pf}, which might be indicative of an endothermic stage, as pointed out before.

Table 3 also presents the average heating rate (β) that has been calculated considering the time needed for reaching T_{Pf} in each experiment. The values obtained (14.1-76.8 ºC·min^{-1}) show a linear increase (R^2=0.97) from P400 to P800.

Table 3. Maximum (T_{Pmax}) and final pyrolysis temperatures (T_{Pf}) measured in the biomass bed, ratio between this maximum temperature and initial temperature of the outer sand bed (T_{S0}), and average heating rate of each experiment (β).

Experiment	T_{Pmax}(ºC)	T_{Pf} (ºC)	T_{Pf}/T_{S0}	β (ºC·min^{-1})
P400	315	315	0.79	14.2
P500	347	332	0.66	25.5
P600	444	425	0.71	51.5
P700	517	492	0.70	57.6
P800	587	556	0.70	76.8

3.3. Pyrolysis products.

The average product yields are shown in Figure 6. The product distribution across temperature is in agreement with those trends previously shown in the literature for similar materials [37,42,43]. For pyrolysis temperatures higher than 325 ºC, the major product fraction is the liquid phase. This fraction reaches around 60 wt. % at the highest temperatures of the experimental range. The solid yield decreases dramatically from 315 to 332 ºC, and reaches values of 20 wt. % at the maximum pyrolysis temperature. Finally, the gas yield (determined by difference and therefore subject to higher uncertainties) slowly increases above 332 ºC, and reaches maximum values of 20 wt. % at the higher end of the temperature interval. The absence of a carrier gas appears to cause a decrease in the gas yields, as pointed out by Crombie and Mašek [44]; however, no clear increases in the char yields can be seen.

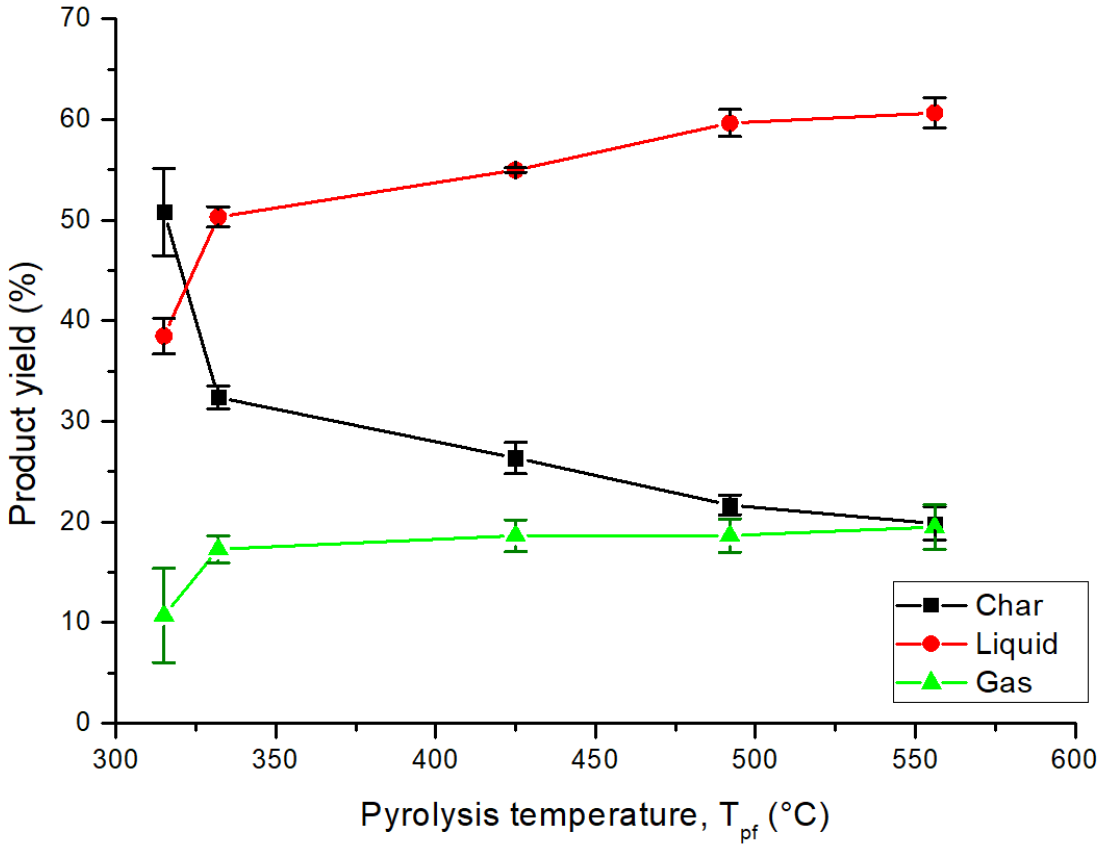

Figure 6. Product yields from pyrolysis.

3.3.1. Solid fraction.

With increasing temperature, the solid product fraction follows the expect trends [45] as evidenced by the analyses shown in Table 4: low moisture contents (hydrophobicity), progressive enrichment in ash content and simultaneous loss of volatiles, and increased fixed C and C content. In fact, the carbon content of the chars produced at the highest temperature is over 90 wt. %. Accordingly, the higher heating values of the chars monotonically increase in the temperature range tested. Finally, the fixed carbon yield, usually taken as an indicator of the efficiency of biomass conversion into char, is comparable to other hardwood chars pyrolyzed at similar temperatures [2,46].

Table 4. Proximate/ultimate analyses, higher heating value (HHV) and fixed carbon yields of the pyrolysis chars.

	units	P400	P500	P600	P700	P800
moisture	wt. %	3.21±0.05	3.91±0.35	2.81±0.61	2.19±0.71	2.49±0.44
ash	wt. %	1.15±0.40	1.92±0.14	2.37±0.16	2.99±0.31	2.84±0.09
volatiles	wt. %	47.11±15.14	28.76±1.75	19.27±0.14	13.80±2.22	9.68±0.92
fixed carbon [a]	wt. %	48.52±14.69	65.41±2.24	75.55±0.63	81.02±1.21	84.99±0.56
C	wt. %	74.65±5.71	78.97±1.86	84.85±4.02	88.19±0.14	90.71±2.13

H[b]	wt. %	5.11±1.01	3.45±0.24	3.02±0.05	2.63±0.02	1.78±0.11
N	wt. %	0.34±0.04	0.48±0.05	0.47±0.05	0.56±0.08	0.56±0.01
O[c]	wt. %	18.70±7.17	15.13±1.93	9.24±4.10	5.57±0.30	4.08±1.94
HHV	$MJ \cdot kg^{-1}$	26.06±1.86	28.94±0.27	30.86±0.82	31.30±0.81	31.36±1.14
Fixed C yield[d]	%	27.30±6.27	22.51±0.19	20.73±1.22	18.11±0.41	17.41±1.25

[a] By difference. [b] Includes moisture hydrogen. [c] O= 100 – C – H – N – S – ash (wt. %). [d] fixed-carbon yield = (char yield) × [(fixed carbon content)/(100 – (ash content)]

3.3.2. Liquid fraction.

Apparently, the liquids obtained show a single phase (no centrifugation was performed to these liquids). Other authors have identified distinct phases in slow pyrolysis liquids [47].

Table 5. Ultimate analyses, higher heating values (HHV), water contents and yields of the pyrolysis liquids.

	units	P400	P500	P600	P700	P800
C	wt. %	25.38	23.70	33.92	32.81	29.58
H[a]	wt. %	9.10	9.42	8.45	8.68	8.87
N	wt. %	0.00	0.00	0.01	0.02	0.03
S	wt. %	n.d.	n.d.	n.d.	n.d.	n.d.
O[b]	wt. %	65.49	66.87	57.60	58.46	61.50
Water content	wt.%	43.53±5.35	41.46±9.28	33.05±0.46	36.94±3.23	39.28±0.19
Water yield	wt. %	16.74±2.20	20.86±4.69	18.17±0.27	22.03±1.99	23.82±0.60
Organics yield	wt.%	21.72±2.83	29.46±4.80	36.81±0.36	37.62±2.40	36.83±1.63
HHV	$MJ \cdot kg^{-1}$	9.74	8.97	12.58	12.54	11.27

[a] Includes moisture hydrogen. [b] O= 100 – C – H – N – S – ash (wt. %).

Results on liquid characterization are presented in Table 5. Compared to the typical values for fast pyrolysis [48,49], the liquid fractions are characterized by a high water content, as highlighted previously by other authors [50]. As a result, relatively low values of HHV are found, and the water yield is over 15 wt. %. However, the high variability of some of these values, as well as the relevant changes in the slopes of the temperature curves shown in Figure 4 around 100 ºC, may suggest that some moisture was incorporated into some biomass samples during their introduction in the fixed bed reactor.

The organics yield (the amount of biomass that is converted into organic liquid compounds, i.e., discounting water content) increases in the first half of the temperature range and reaches constant value of around 36-38 wt. % at the highest temperatures.

3.3.3. Gas fraction.

Figure 7 shows the evolution of gas composition as a function of temperature. The graph includes the last analyses for each experiment (P400 to P800), when both the bed temperatures and the gas compositions

remain more or less constant (the latter, because gas generation ceases). Curves from Figure 7 can provide an idea of the evolution of gas composition during slow pyrolysis; however, the temperature values are subject to considerable uncertainty, because the chromatograph system is located after the condensation train, and therefore there is a significant delay in gas measurements. Moreover, this delay cannot be determined because no carrier gas was used, and therefore gas flowrates are widely variable over an experiment.

The gas is mainly composed of CO_2, CO, CH_4, H_2 and minor amounts of light hydrocarbons. At the beginning of each experiment, CO_2 is the main gas detected with only small amounts of CO. As the pyrolysis temperatures rise, the concentration of CO, CH_4 and light hydrocarbons gradually increase [34], reaching maximum concentrations before 500 ºC (CO, CH_4) and after this temperature for C_2s (C_2H_4, C_2H_6). Apparently, high temperatures cause the production of high levels of methane if compared to literature values [37]. This fact can be attributed to the absence of a gas carrier [44]. CO_2 remains the main gas species within the entire range, although hydrogen (which is detected in significant amounts beyond 400 ºC) increases rapidly at high temperatures, reaching almost 40% vol. at around 550 ºC.

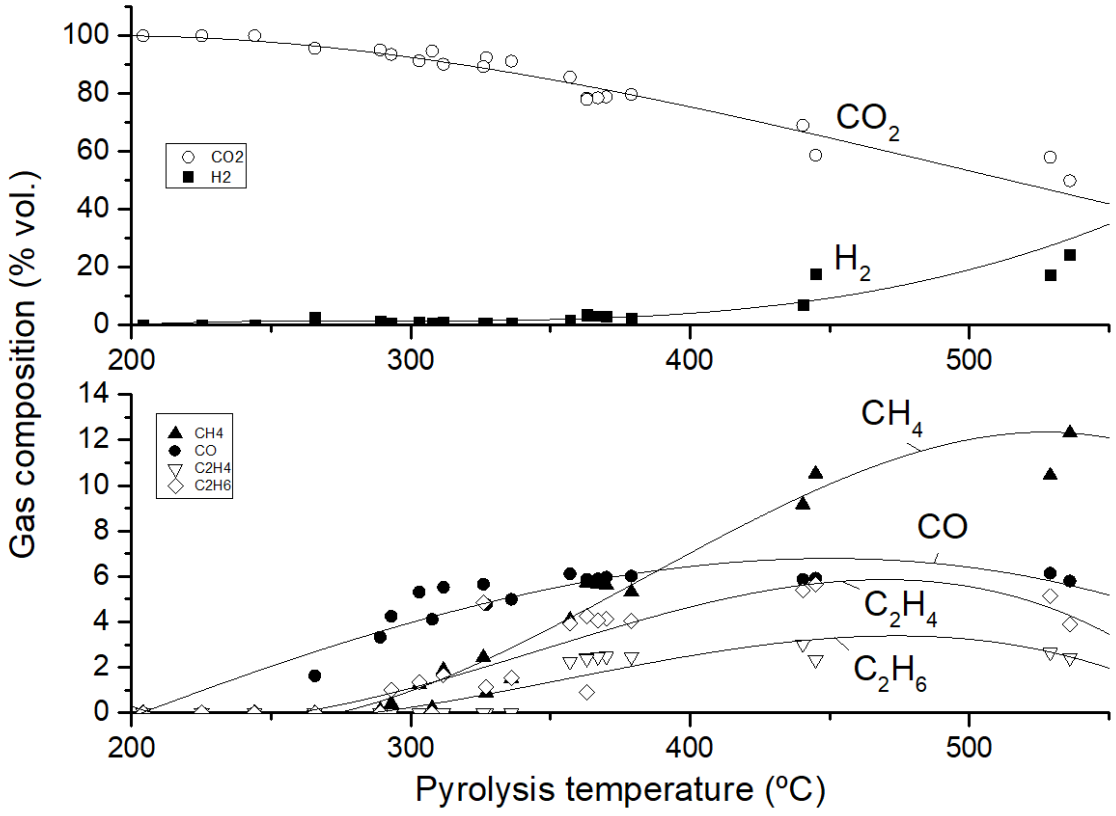

Figure 7. Evolution of gas composition as a function of temperature.

3.4. Heat for pyrolysis (Q_P).

The evolution of heats for biomass pyrolysis, as estimated by the proposed procedure, are shown in Figures 8a-8f as a function of pyrolysis temperature. Final pyrolysis temperatures, T_{Pf}, are also shown, together with additional relevant points (T_a, T_b) that will be further discussed. T_{Pf} values can be easily determined because beyond these temperatures (not shown in the Figures), Q_P suddenly increases at a high and constant rate, which is indicative of heating of the char material and coincides with slow, steady temperature increases in the char bed.

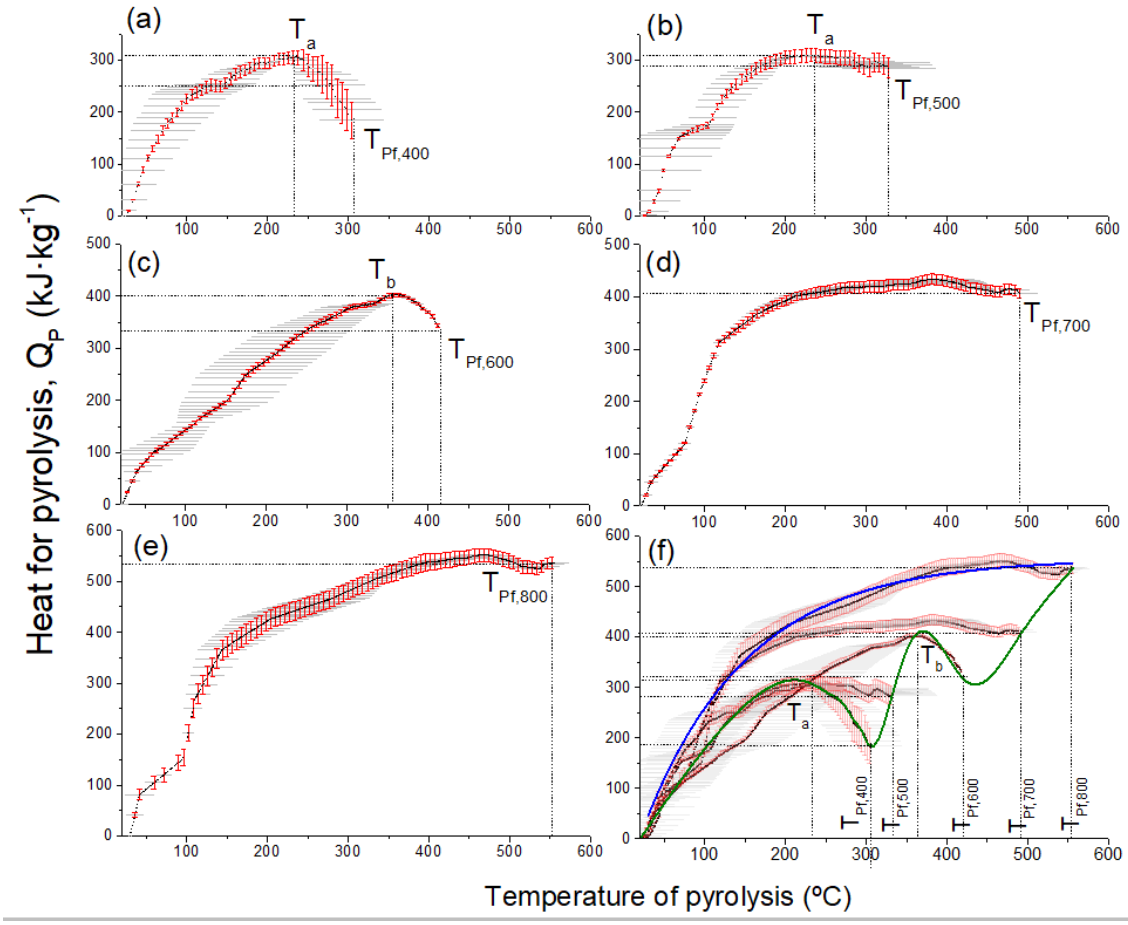

Figure 8 (a-e) Q_P curves for experiments P400 to P800 locating relevant temperatures; (f) all experimental data with: (····) superimposed composite curve representing Q_P at very slow heating rates; (----) exponential fit of P800 data representative of Q_P at high heating rates. Both vertical (red) and horizontal error bars (gray) are included. All the curves have been represented at identical scale for better comparison.

It must be kept in mind that calculated Q_P values are associated to the central bed temperature. As explained before, it can be reasonably assumed that the temperature of the char bed in the final stage of a pyrolysis experiment (at the end of each curve) is nearly uniform, especially if temperature overshoots are small or absent. Therefore, in these cases, T_P can be assumed as really representative of the whole char bed. However, at the beginning of each curve, high temperature differences can be found in the radial profile of the bed; thus, T_P in these cases might not be as representative of the average bed temperature (that would be higher). This temperature difference is higher when applying high heating rates (higher external temperatures).

Table 6. Relevant temperatures identified from Figure 8.

Experiment	Point	T (ºC)	Q_P (kJ·kg^{-1})
P400	T_a	235	305
	$T_{Pf,400}$	315	185
P500	T_a	235	305
	$T_{Pf,500}$	332	284
P600	T_b	360	403
	$T_{Pf,600}$	425	310
P700	$T_{Pf,700}$	492	407
P800	$T_{Pf,800}$	556	536

Keeping these limitations in mind, final pyrolysis temperatures (T_{Pf}) and other relevant temperatures (T_a and T_b) where thermal effects from pyrolysis are evident are graphically identified in Figure 8 and summarized in Table 6. Examination of these points show, for instance, that experiments P400 and P600 present maximum values of Q_P before pyrolysis is finished (points T_a and T_b, corresponding to 305 kJ·kg^{-1} at 235 ºC and 403 kJ·kg^{-1} at 360 ºC, respectively) evidencing two exothermic stages peaking at those temperatures. Afterwards, the final estimated values for Q_P are 185 and 310 kJ·kg^{-1} respectively. T_a can also be identified in Figure 8b (experiment P500).

The values for Q_P range between minimum and maximum values of 185 and 536 kJ·kg^{-1}, depending on the final temperature of each experiment. Compared to that from the literature, the values of Q_P obtained in this work are substantially lower than those reported in laboratory scale reactors, such as fluidized bed systems (780-3300 kJ·kg^{-1}, [7,16,17]) or screw reactors (1100-1600 kJ·kg^{-1} [11]). The reason for these differences can be attributed to the inherent use of very small particle sizes in the case of fluidized bed reactors, and to the very high gas flow rates in both types of reactors. Small particle sizes and high carrier gas flowrates are known to substantially increase the overall endothermic behavior of pyrolysis [2,26,51]. In the case of small particles, the occurrence of intraparticle reactions is dramatically reduced, whereas for high gas flowrates,

vapor-solid interactions are hindered by the lower residence time of the volatiles. Both aspects negatively impact the exothermicity, although the latter effect seems to be far more important for wood materials [3]. Indeed, the literature data reviewed here have in common the use of very high flowrates of inert gases. In the case of a screw reactor for torrefaction [9] operating in a temperature range between 270 and 300 ºC and using low nitrogen flowrates as inert gas (more than ten times lower N_2/biomass feed ratio than in reference [11]), Ohliger et al. reported Q_P values between 249 and 400 $kJ \cdot kg^{-1}$, very similar to those reported in this work within the same temperature range. The strong influence of gas flowrate, as reviewed by Antal and Grönli, might even determine the sign of ΔH_P (exo/endothermic).

The first stages of some curves in Figure 8, and in general values of Q_P at low temperatures, show great temperature differences both in the horizontal error bars (differences between replicates) and also between experiments. The poor reproducibility at low temperatures may be caused by inhomogeneity in bed packing, residual moisture evaporation and, specially, in the uncertainties caused by the overlapping of thermal effects (including moisture evaporation, decomposition reactions, formation of vapor products, and their recondensations and evaporations) as a result of the presence of high temperature gradients. In contrast, high temperature experiments show good reproducibility.

The examination of the curves from Figure 8 allows drawing some conclusions about the evolution of Q_P. For instance, Figure 8a reveals the existence of an exothermic stage in experiment P400, which ranges between 235 and 315 ºC approximately (between T_a and $T_{Pf,400}$). This observation is in accordance with the exothermic stage identified in the DSC curve at similar temperatures, and also identified in the time derivatives dT_P/dt presented in Figure 5 (beginning at 225 ºC). However, experiment P500 (Figure 8b) shows that at slightly higher temperatures of the bed, the exothermic effect is partially hindered by a subsequent endothermic stage that can be ascribed to the narrow temperature range between 315 and 332 ºC. Again, it has to be remarked that temperatures in this region are subject to significant uncertainty.

Figure 8c shows again an exothermic stage, starting at 360 ºC and up to 425 ºC. Finally, Figures 8d and 8e, corresponding to experiments P700 and P800, do not show marked fluctuations, but reveal increasingly higher heat demand for pyrolysis and therefore the occurrence of an endothermic stage up to the maximum temperature of 556 ºC. The absence of local minima or maxima in these two curves reflect the existence of high temperature gradients in the bed, and therefore the simultaneous overlapping of thermal phenomena (exo and endothermic) that become individually undistinguishable. A similar observation has been made very recently by Di Blasi and co-workers [52] for thermally severe heating conditions, in which exothermic

heat evolved within a fixed bed preheats the biomass to higher decomposition temperatures. Finally, it must be also mentioned that, at the beginning of some experiments (P500, P700 and P800) the steeper slopes of the curves just after 100 ºC suggests water evaporation and therefore the presence of some moisture in the samples.

As could be expected, significant variations in the heat requirements of a fixed bed pyrolysis reactor can be found, depending on the heating rate and final temperature. More importantly, experimental data show that the overall heat requirements of such reactors do not necessarily always increase with temperature. Noticeable exothermic events inside the reactor might influence the final temperature and therefore the final pyrolysis yields [53], and thus need to be determined as accurately as possible in order to avoid runaway reactions and/or unexpected product yields at pilot or industrial scale.

3.4.1. Evolution of Q_P at slow pyrolysis conditions

A composite Q_P curve built using the experimental points summarized in Table 6 can be seen as an approximation to illustrate the thermal events that would occur during fixed bed pyrolysis of wood chips at very slow heating rates (i.e., with nearly homogeneous radial profiles of bed temperatures throughout the experiment). The composite curve can be seen in Figure 8f. This graph coincides with the following sequence of thermal events, as reviewed by Di Blasi et al. [3]: (i) an exothermic stage attributed to hemicellulose decomposition that, in the conditions of this study, begins around 235 ºC and ends at 315 ºC approximately; (ii) an endothermic stage mainly caused by the simultaneous decomposition of cellulose and lignin, peaking at 360 ºC approximately; and (iii) another exothermic region linked to further decomposition of the lignin fraction (peak at around 425 ºC) followed by a continuous increase in heat demand up to 556 ºC. Besides the good qualitative agreement with literature data, numerical estimations of the evolution of Q_P with temperature are provided here.

If qualitatively compared to DSC data (Figure 3), the composite curve for Q_P of Figure 8f is almost equal below 200 ºC, but shows significant differences at higher temperatures. In DSC, there is a continuous exothermic stage between 270 and 445 ºC, whereas in the fixed bed, the exothermic effect begins at somewhat lower temperatures (235 ºC), and an intermediate endothermic interval is found (315–332 ºC). Discrepancies between both curves are attributable to the very different extent of secondary interactions in both systems (different vapor residence times inside the biomass particles and the absence of interparticle

interactions in the case of DSC) and suggest that, when measuring heat effects in DSC analysis, experimental conditions might be not representative of those of practical interest.

3.4.2. Evolution of Q_P at high heating rates

As said before, Figure 8 suggests that under our experimental conditions, increasingly higher heating rates (or fluxes) cause 'blurring' of the observed exothermic stages, which overlap with endothermic effects. This might be the case, for instance, of fixed beds externally heated by high heat fluxes, or continuous screw reactors where heating rates are relatively high [9] while biomass particle sizes are almost identical to the ones used in this work (dry wood chips). Given the similarities, the experiment performed at high external temperature and heating rate (P800) might be a good reference for Q_P in screw reactors using low sweeping gas flowrates. The following exponential equation describes with reasonable accuracy the estimated values of heat for pyrolysis (R^2=0.965) up to 556 ºC and could be an approximation for the mentioned operational conditions.

$$Q_P(T) = 554.7 - 641.3 \cdot e^{-0.00774 \cdot T}$$ (T in ºC, Q_P in kJ·kg^{-1} dry biomass) Equation 6

The obtained curve is qualitatively similar in shape to those reported by Van de Velden et al. [13] for various biomasses in a TGA system with high heating rates of 100 K·min^{-1}, and gives slightly higher values of the heat for pyrolysis.

3.5. Heat of pyrolysis (ΔH_P).

As noted before, in order to obtain an estimation of apparent enthalpy of pyrolysis ΔH_P the effect of the sensible heat must be subtracted. Using the experimental char yields from Figure 6, a sensible heat curve $Q_S(T)$ was built and then used to calculate the evolution of ΔH_P with temperature (Equation 7):

$$\Delta H_P(T) = Q_P(T) - Q_S(T)$$ Equation 7

In accordance to the two different assumptions for Q_P previously described (high and low heating rates/fluxes), two different ΔH_P curves ('fast' and 'slow') are displayed in Figure 9a.

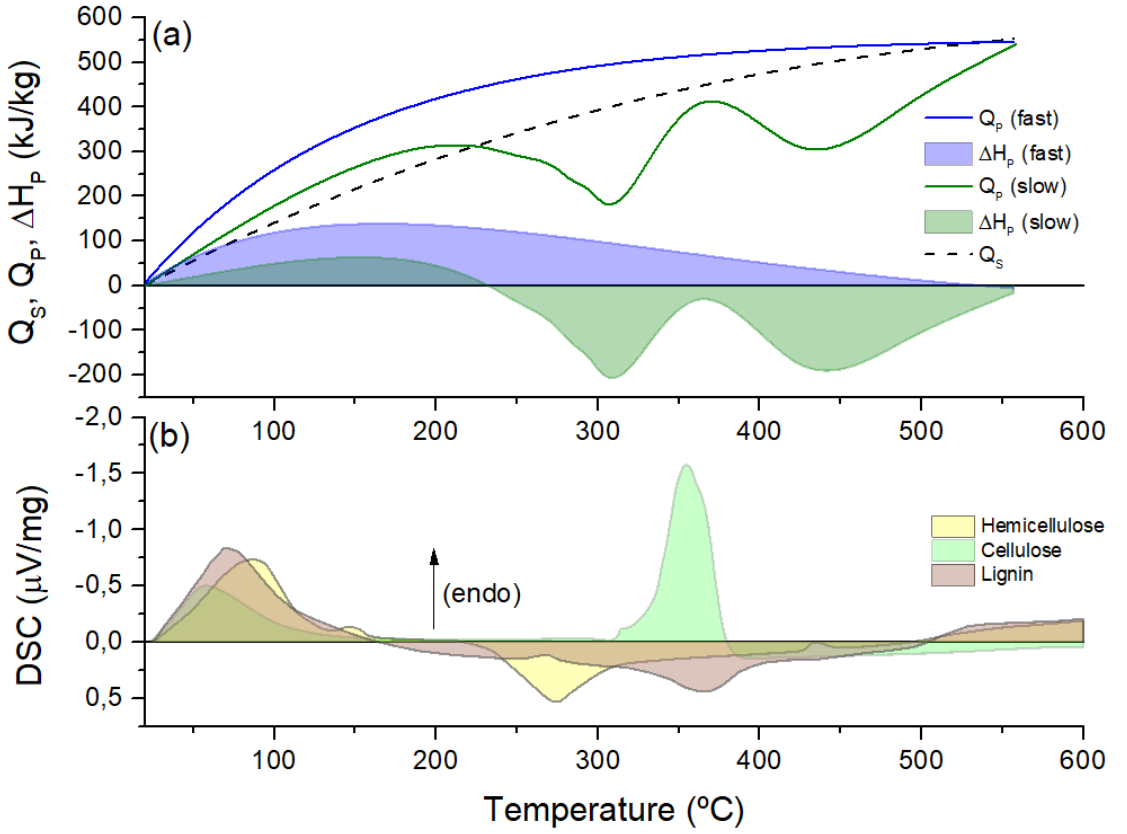

Figure 9. (a) Estimated curves for heat of pyrolysis (ΔH_P) resulting from subtraction of sensible heat, Q_S, from Q_P (also shown). 'Fast' and 'slow' heating conditions represent previous assumptions as depicted in Figure 8. (b) DSC curves of hemicellulose, cellulose and lignin pyrolysis (modified from Yang et al. [54]) are represented for comparison.

Again, comparison of both curves reveals that significant changes for ΔH_P values can be found under different experimental conditions, as reflected in the literature. It can be seen that, under high heat fluxes, ΔH_P is endothermic in the entire temperature range with maximum values of around 140 kJ·kg^{-1}, whereas under slow heating rates, there is a transition from endothermic to exothermic behavior around 230 ºC, and the exothermic character is maintained at any higher temperature with two local minima (-205 and -190 kJ·kg^{-1}, respectively) that can be correlated to the thermal events previously described, therefore corresponding to the degradation of the wood constituents.

Moreover, and as seen in Figure 9b, these observations remarkably agree with the temperature intervals reported for the decomposition of individual components of wood in TGA-DSC in the well-known work by Yang et al [54].

ΔH_P values from this work are similar to most of the literature results reported in Table 1. Considering the same raw material (beech wood), the values reported by van der Stelt [25] and Ohliger [9] show very good agreement in the torrefaction temperature range. The same applies to results given by the model developed by Bates and Ghoniem [4], who also reported increased exothermic character with increasing temperature in the torrefaction range (<300 ºC). At higher pyrolysis temperatures, the values reported by Rath [24] and Gómez [27] in DSC analysis are also very similar.

3.6. Temperature range for pyrolysis self-sustainability

Self-sustainability of pyrolysis is a matter of concern for practical systems [55]. Crombie and Mašek [44], comparing experimentally determined gas compositions to literature values on heat for pyrolysis, concluded that pyrolysis could be maintained above 450 ºC. The reviewed literature values for Q_P ranged between 6-15% of the biomass HHV (including for instance fluidized bed pyrolysis, with much higher energy requirements) and are therefore conservative. Under the operational conditions of this study, Q_P is estimated as less than 3% of HHV. In our work, the high uncertainties in gas flowrates and compositions do not allow calculating gas energy contents; however, the mentioned work by Crombie and Mašek [44] also provides a good reference for comparison with Q_P: experiments performed with wood pellets and without using a gas carrier gave gas energy contents between 0.29-1.89 $MJ \cdot kg^{-1}$ of biomass (350-650 ºC). Under slow pyrolysis conditions and for dry biomass, the self-sustainability criteria could be even met at the lower temperature of 350 ºC. At higher temperatures, the excess heat from pyrolysis gases could be available for partial drying.

4. Conclusions

For wood pyrolysis, the sequences of thermal events previously described in the literature, probably associated to the decomposition of the individual components of wood, have been verified in a lab-scale experimental system. Moreover, measurements of the evolution of heat for pyrolysis and enthalpy of pyrolysis are provided:

- For Q_P, values of around 550 kJ/kg of dry biomass are found for final pyrolysis temperatures around 550 ºC. The evolution of Q_P is different upon ‘slow’ or ‘fast’ heating rates (low or high external heat fluxes) applied. Slow heating reveals temperature intervals where exothermic effects are manifest, which lower the energy requirements of pyrolysis.ΔH_P is endothermic under high heat fluxes in the entire temperature range, with maximum value of around 150 kJ/kg. Under slow heating rates, there

is a transition from endothermic to exothermic behavior around 230 ºC, and the exothermic character is maintained at any higher temperature with two local minima (-150 and -190 kJ/kg, respectively) that can be correlated to the degradation of the wood constituents.

- These results are obtained under conditions that could be relevant to the industrial practice for the combined production of biochar and pyrolysis liquid, whereas some other techniques such as DSC might not be as representative of such experimental conditions.
- There is no obvious relationship between the characteristics of the lumped products and the evolution of heat during pyrolysis; rather, the mentioned correlation between thermal events and the decomposition of the individual wood components (hemicellulose, cellulose and lignin) is found.
- The experimental system can be potentially used to investigate the influence of relevant parameters, such as moisture content, gas residence time, particle size, reaction atmosphere or heating rate, and catalyst addition, amongst others, in the evolution of heat. Nevertheless, further improvements could be made to the experimental system; for instance, better reproducibility and precision at the beginning of experiments should be achieved. Additionally, measurement of thermal fields of the reactor (and not only one representative temperature) would be advisable.

5. Acknowledgment

This work was supported by a grant from University of Zaragoza (JIUZ-2016-TEC-01). The authors are grateful to Olga Marín for her valuable help in product characterization.

6. References

[1] Garcia-Nunez JAA, Pelaez-Samaniego MRR, Garcia-Perez ME, Fonts I, Abrego J, Westerhof RJMJM, et al. Historical Developments of Pyrolysis Reactors: A Review. Energy & Fuels 2017;31:5751–75. doi:10.1021/acs.energyfuels.7b00641.

[2] Antal Jr MJ, Grønli M. The Art, Science, and Technology of Charcoal Production. Ind Eng Chem Res 2003;42:1619–40. doi:10.1021/ie0207919.

[3] Di Blasi C, Branca C, Galgano A. On the Experimental Evidence of Exothermicity in Wood and Biomass Pyrolysis. Energy Technol 2017;5:19–29. doi:10.1002/ente.201600091.

[4] Bates RB, Ghoniem AF. Biomass torrefaction: Modeling of reaction thermochemistry. Bioresour Technol 2013;134:331–40. doi:10.1016/j.biortech.2013.01.158.

[5] Branca C, Di Blasi C. A summative model for the pyrolysis reaction heats of beech wood. Thermochim Acta 2016;638:10–6. doi:10.1016/j.tca.2016.06.006.

[6] Piskorz J, Peacocke GVC, Bridgwater A V. IEA Pyrolysis Fundamentals Review. In: Bridgewater, A., Czernik, S., Diebold, J., Meier, D., Oasmaa, A., Peacocke, C., Piskorz, J., Radlein D, editor. Fast Pyrolysis Biomass A Handb., Newbury, U.K.: CPL Scientific Publishing Services Limited; 1999, p. 33–50.

[7] Daugaard DE, Brown RC. Enthalpy for Pyrolysis for Several Types of Biomass. Energy & Fuels 2003;17:934–9. doi:10.1021/ef020260x.

[8] Reed TB, Gaur S. The high heat of fast pyrolysis for large particles. In: Bridgwater A V., Boocock DGB, editors. Dev. Thermochem. Biomass Convers., Blackie Academic & Professional; 1997, p. 97–103.

[9] Ohliger A, Förster M, Kneer R. Torrefaction of beechwood: A parametric study including heat of reaction and grindability. Fuel 2013;104:607–13. doi:10.1016/j.fuel.2012.06.112.

[10] Ábrego J, Plaza D, Luño F, Atienza-Martínez M, Gea G. Pyrolysis of cashew nutshells: Characterization of products and energy balance. Energy 2018. doi:10.1016/j.energy.2018.06.011.

[11] Yang H, Kudo S, Kuo H-P, Norinaga K, Mori A, Mašek O, et al. Estimation of Enthalpy of Bio-Oil Vapor and Heat Required for Pyrolysis of Biomass. Energy & Fuels 2013;27:2675–86. doi:10.1021/ef400199z.

[12] He F, Yi W, Bai X. Investigation on caloric requirement of biomass pyrolysis using TG-DSC analyzer. Energy Convers Manag 2006;47:2461–9. doi:10.1016/j.enconman.2005.11.011.

[13] Van de Velden M, Baeyens J, Brems A, Janssens B, Dewil R. Fundamentals, kinetics and endothermicity of the biomass pyrolysis reaction. Renew Energy 2010;35:232–42. doi:10.1016/j.renene.2009.04.019.

[14] Bilbao R, Mastral JF, Ceamanos J, Aldea ME. Modelling of the pyrolysis of wet wood. J Anal Appl Pyrolysis 1996;36:81–97. doi:10.1016/0165-2370(95)00918-3.

[15] Manyà JJ, Laguarta S, Ortigosa MA. Study on the Biochar Yield and Heat Required during Pyrolysis of Two-Phase Olive Mill Waste. Energy & Fuels 2013;27:5931–9. doi:10.1021/ef4012388.

[16] Berruti FM, Ferrante L, Briens CL, Berruti F. Pyrolysis of cohesive meat and bone meal in a bubbling fluidized bed with an intermittent solid slug feeder. J Anal Appl Pyrolysis 2012;94:153–62. doi:10.1016/J.JAAP.2011.12.003.

[17] Xu R, Ferrante L, Briens C, Berruti F. Flash pyrolysis of grape residues into biofuel in a bubbling

fluid bed. J Anal Appl Pyrolysis 2009;86:58–65. doi:10.1016/J.JAAP.2009.04.005.

[18] Kodera Y, Kaiho M. Model Calculation of Heat Balance of Wood Pyrolysis. J Japan Inst Energy 2016;95:881–9. doi:10.3775/jie.95.881.

[19] Hosokai S, Matsuoka K, Kuramoto K, Suzuki Y. Practical estimation of reaction heat during the pyrolysis of cedar wood. Fuel Process Technol 2016;154:156–62. doi:10.1016/j.fuproc.2016.08.027.

[20] Ábrego J, Sánchez JL, Arauzo J, Fonts I, Gil-Lalaguna N, Atienza-Martínez M. Technical and energetic assessment of a three-stage thermochemical treatment for sewage sludge. Energy & Fuels 2013;27:1026–34. doi:10.1021/ef3018095.

[21] Atienza-Martínez M, Ábrego J, Mastral JF, Ceamanos J, Gea G. Energy and exergy analyses of sewage sludge thermochemical treatment. Energy 2018;144. doi:10.1016/j.energy.2017.12.007.

[22] Klason P. Versuch einer Theorie der Trockendestillation von Holz. I. J Für Prakt Chemie 1914;90:413–47. doi:10.1002/prac.19140900127.

[23] Roberts AF. The Heat of Reaction During the Pyrolysis of Wood. Combust Flame 1971;17:79–86. doi:10.1016/S0010-2180(71)80141-4.

[24] Rath J, Wolfinger MG, Steiner G, Krammer G, Barontini F, Cozzani V. Heat of wood pyrolysis. Fuel 2003;82:81–91. doi:10.1016/S0016-2361(02)00138-2.

[25] Van Der Stelt MJC. Chemistry and reaction kinetics of biowaste torrefaction. Eindhoven University of Technology, n.d. doi:10.6100/IR695294.

[26] Basile L, Tugnoli A, Stramigioli C, Cozzani V. Thermal effects during biomass pyrolysis. Thermochim Acta 2016;636:63–70. doi:10.1016/j.tca.2016.05.002.

[27] Gomez C, Velo E, Barontini F, Cozzani V. Influence of Secondary Reactions on the Heat of Pyrolysis of Biomass. Ind Eng Chem Res 2009;48:10222–33. doi:10.1021/ie9007985.

[28] Chen Q, Yang R, Zhao B, Li Y, Wang S, Wu H, et al. Investigation of heat of biomass pyrolysis and secondary reactions by simultaneous thermogravimetry and differential scanning calorimetry. Fuel 2014. doi:10.1016/j.fuel.2014.05.092.

[29] Radovich JM. Technical Considerations of Biomass Conversion Processes. Biomass Convers. Process. Energy Fuels, Boston, MA: Springer US; 1981, p. 377–98. doi:10.1007/978-1-4757-0301-6_20.

[30] Grønli MG. A theoretical and experimental study of the thermal degradation of biomass. 1996.

[31] Hankalin V, Ahonen T, Raiko R. On Thermal Properties of a Pyrolysing Wood Particle. Finnish-Swedish Flame Days 2009, Naantali, Finland.: 2009.

[32] Comesaña JA, Nieström M, Granada E, Szlek A. TG-DSC analysis of biomass heat capacity during pyrolysis process. J Energy Inst 2013;86:153–9. doi:10.1179/1743967112Z.00000000055.

[33] Dupont C, Chiriac R, Gauthier G, Toche F. Heat capacity measurements of various biomass types and pyrolysis residues. Fuel 2014;115:644–51. doi:10.1016/j.fuel.2013.07.086.

[34] Khalil RA, Mészáros E, Grønli MG, Várhegyi G, Mohai I, Marosvölgyi B, et al. Thermal analysis of energy crops: Part I: The applicability of a macro-thermobalance for biomass studies. J Anal Appl Pyrolysis 2008;81:52–9. doi:10.1016/J.JAAP.2007.08.004.

[35] Balme Q, Lemont • F, Rousset • F, Sedan • J, Charvin • P, Bondroit • J, et al. Design, calibration and testing of a new macro-thermogravimetric analyzer. J Therm Anal Calorim n.d.;132. doi:10.1007/s10973-018-7118-x.

[36] Schröder E. Experiments on the pyrolysis of large beechwood particles in fixed beds. J Anal Appl Pyrolysis 2004;71:669–94. doi:10.1016/j.jaap.2003.09.004.

[37] di Blasi C, Branca C, Masotta F, Biase E De, Tecchio V, Di Blasi C, et al. Experimental Analysis of Reaction Heat Effects during Beech Wood Pyrolysis. Energy & Fuels 2013;27:2665–74. doi:10.1021/ef4001709.

[38] Outotec Research. HSC chemistry 9.0, Chemical reaction and equilibrium software with thermochemical database and simulation module 2016. https://www.outotec.com/products/digital-solutions/hsc-chemistry/ (accessed May 30, 2018).

[39] Hrablay I, Jelemenský Ľ. Kinetics of thermal degradation of wood biomass. Chem Pap 2014;68:1725–38. doi:10.2478/s11696-014-0622-y.

[40] He F, Yi W, Bai X. Investigation on caloric requirement of biomass pyrolysis using TG–DSC analyzer. Energy Convers Manag 2006;47:2461–9. doi:10.1016/j.enconman.2005.11.011.

[41] Ciuta S, Patuzzi F, Baratieri M, Castaldi MJ. Enthalpy changes during pyrolysis of biomass: Interpretation of intraparticle gas sampling. Appl Energy 2018;228:1985–93. doi:10.1016/J.APENERGY.2018.07.061.

[42] Neves D, Thunman H, Matos A, Tarelho L, Gómez-Barea A. Characterization and prediction of biomass pyrolysis products. Prog Energy Combust Sci 2011;37:611–30. doi:10.1016/j.pecs.2011.01.001.

[43] Di Blasi C. Modeling chemical and physical processes of wood and biomass pyrolysis. Prog Energy Combust Sci 2008;34:47–90. doi:10.1016/j.pecs.2006.12.001.

[44] Crombie K, Mašek O. Investigating the potential for a self-sustaining slow pyrolysis system under varying operating conditions. Bioresour Technol 2014;162:148–56. doi:10.1016/j.biortech.2014.03.134.

[45] Tintner J, Preimesberger C, Pfeifer C, Soldo D, Ottner F, Wriessnig K, et al. Impact of pyrolysis temperature on charcoal characteristics. Ind Eng Chem Res 2018:acs.iecr.8b04094. doi:10.1021/acs.iecr.8b04094.

[46] Antal Jr MJ, Allen SG, Dai X, Shimizu B, Tam MS, Grønli M. Attainment of the Theoretical Yield of Carbon from Biomass. Ind Eng Chem Res 2000;39:4024–31. doi:10.1021/ie000511u.

[47] Phan AN, Ryu C, Sharifi VN, Swithenbank J. Characterisation of slow pyrolysis products from segregated wastes for energy production. J Anal Appl Pyrolysis 2008;81:65–71. doi:10.1016/j.jaap.2007.09.001.

[48] Oasmaa A, Czernik S. Fuel oil quality of biomass pyrolysis oils - State of the art for the end user. Energy & Fuels 1999;13:914–21. doi:10.1021/ef980272b.

[49] Oasmaa A, Meier D. Bio-oil - Characterisation, analysis, norms & standards. 2000.

[50] Bridgwater A V, Carson P, Coulson M. A comparison of fast and slow pyrolysis liquids from mallee. Int J Glob Energy Issues n.d.;x x. doi:10.1504/IJGEI.2007.013655.

[51] Mok WSL, Antal Jr MJ, Szabo P, Varhegyi G, Zelei B. Formation of charcoal from biomass in a sealed reactor. Ind Eng Chem Res 1992;31:1162–6. doi:10.1021/ie00004a027.

[52] Di Blasi C, Branca C, Galgano A, Autiero G. Analysis of the Pyrolytic Runaway Dynamics during Agricultural Waste Conversion 2018. doi:10.1021/acs.energyfuels.8b01907.

[53] Di Blasi C, Branca C, Sarnataro FE, Gallo A. Thermal runaway in the pyrolysis of some lignocellulosic biomasses. Energy and Fuels 2014;28:2684–96. doi:10.1021/ef500296g.

[54] Yang H, Yan R, Chen H, Lee DH, Zheng C. Characteristics of hemicellulose, cellulose and lignin pyrolysis. Fuel 2007;86:1781–8. doi:10.1016/j.fuel.2006.12.013.

[55] Rollinson AN, Oladejo JM. 'Patented blunderings', efficiency awareness, and self-sustainability claims in the pyrolysis energy from waste sector. Resour Conserv Recycl 2019;141:233–42. doi:10.1016/J.RESCONREC.2018.10.038.

Figure 1. Schematic diagram of different magnitudes used to describe the energy requirements of the biomass pyrolysis process, and their relationships.

Figure 2. Schematic figure of the experimental system.

Figure 3. (a) TGA-DSC curves for a single beech wood chip. (b) QP based on integration of the DSC data (not taking into account the peak from biomass moisture)